Construction and testing of the wavefront sensor camera for the new MMT adaptive optics system

P.C. McGuire, T.A. Rhoadarmer[a], M. Lloyd-Hart, J.C. Shelton[b], M.P. Lesser, J.R.P. Angel, G.Z. Angeli, J.M. Hughes, B.C. Fitz-Patrick, M.L. Rademacher, P. Schaller, M.A. Kenworthy, F.P. Wildi, J.G. Capara[c], D.B. Ouellette,
CENTER FOR ASTRONOMICAL ADAPTIVE OPTICS,
STEWARD OBSERVATORY, UNIVERSITY OF ARIZONA, Tucson, AZ 85721
[a]now at Starfire Optical Range, Kirtland Airforce Base, New Mexico 87117-5776
[b]now at W.M. Keck Observatory, Kamuela, Hawaii.
[c]now at Raytheon Defense Systems, Tucson, Arizona.

ABSTRACT

This paper describes the construction and testing of the Shack-Hartmann wavefront sensor (WFS) camera for the new MMT adaptive optics system. Construction and use of the sensor is greatly simplified by having the 12 × 12 lenslet array permanently glued to the detector array, obviating the need for any further realignment. The detector is a frame transfer CCD made by EEV with 80 × 80 pixels, each 24 microns square, and 4 output amplifiers operated simultaneously. 3 × 3 pixel binning is used to create in effect an array of quad-cells, each centered on a spot formed by a lenslet. Centration of the lenslet images is measured to have an accuracy of 1 μm (0.02 arcsec) rms. The maximum frame rate in the binned mode is 625 Hz, when the rms noise is 4.5 – 5 electrons. In use at the telescope, the guide star entering the wavefront sensor passes through a 2.4 arcsec square field stop matched to the quad-cell size, and each lenslet samples a 54 cm square segment of the atmospherically aberrated wavefront to form a guide star image at a plate scale of 60 μm/arcsec. Charge diffusion between adjacent detector pixels is small: the signal modulation in 0.7 arcsec seeing is reduced by only 10% compared to an ideal quad-cell with perfectly sharp boundaries.

Keywords: wavefront sensor camera, WFS, Shack-Hartmann, pixel transfer function,WFS transfer curve, turbulence plate, noise sensitivity, CCD, lenslet array, CCD read noise

1. SHACK-HARTMANN WAVE FRONT SENSOR

The new MMT, with its 6.5 meter diameter reflector upgrade, will soon see first light, with adaptive optics (AO) first light to follow soon thereafter. Herein, we describe the construction and testing of the MMT WFS camera. More details are given by Rhoadarmer.[1]

Integral to any AO system is the wavefront sensor (WFS), as the WFS serves as the eyes of an adaptive optics system.[2–5] It collects information about the phase aberrations in an incoming wavefront which is then used by the reconstruction algorithm to control the deformable mirror (DM). The most popular WFS used in real-time AO systems, including the AO system for the new MMT, is the Shack-Hartmann WFS, due to its simplicity of construction and operation. It only has two basic components, a lenslet array and a CCD camera, that work together to measure the slope of an incoming wavefront.

One of the most common detector configurations uses a 2 × 2 quad-cell for each subaperture.[6] The WFS cameras in the AO systems at Starfire Optical Range,[7] Mt. Wilson,[8] and Keck[9] are among the examples with quad-cells and well-centered spots that are operational now. For each quad-cell, one determines the local slope of the wavefront across each lenslet subaperture by taking the imbalance in counts between the two halves of the quad-cell. By combining the data from all of the subapertures, an estimate of the wavefront can be determined. This estimate is then used to adjust the shape of the DM. The major drawback of using 2 × 2 quad-cells instead of 4 × 4 pixel configurations is the limitation of dynamic range to ±1 wave of tilt,[6] but dynamic range is not usually an issue after the AO loop is closed. Therefore, 2 × 2 quad-cells are usually employed due to the high speed of CCD read-out.

Other author information:
P.C.M.: EMAIL:mcguire@as.arizona.edu TELEPHONE:(520)621-7870,
T.A.R.: EMAIL:rhoadart@plk.af.mil

Part of the SPIE Conference on Adaptive Optics Systems and Technology
Denver, Colorado • July 1999
SPIE Vol. 3762 • 0277-786X/99/$10.00

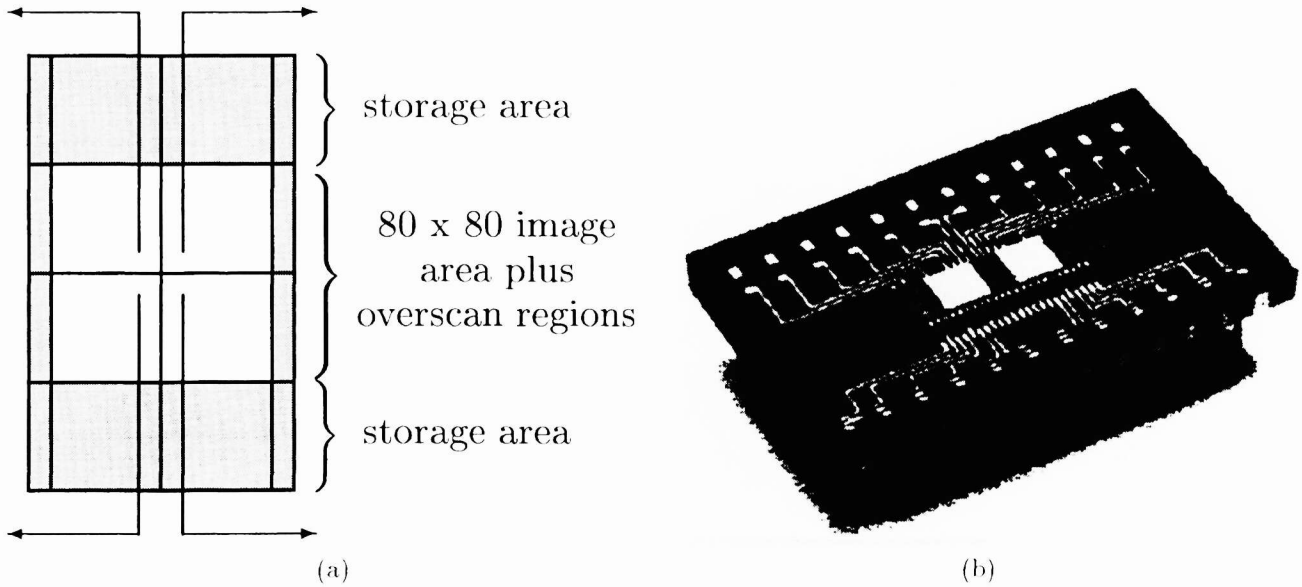

Figure 1. The EEV CCD39A device. Figure (a) depicts a diagram of the chip structure with the arrows showing the direction of readout for the four frame quadrants. The unshaded regions in the middle correspond to the image quadrants. The shaded regions on the top and bottom of the chip are the frame-transfer storage areas and the shaded regions on each side are the 7 overscan rows. Figure (b) is an image of the device, with the frame transfer areas showing as large white squares and the sensitive area in the narrow rectangle between the white squares.

The WFS camera for the MMT AO system contains a CCD39A device manufactured by EEV.[10] This detector is a thinned, back-illuminated device with a square 80 × 80 array format and 24 μm × 24 μm pixels. The active area is 100% and the quantum efficiency in the visible is greater than 80%. The 4-port, split-frame transfer architecture has been optimized for high frame rates, up to 1 kHz, and low read noise, 3 to 6 electrons, when operated at −50°C. A diagram and picture of the chip are shown in figure 1.

For the first generation of the AO system, the WFS geometry consists of a 12 × 12 square array of square subapertures. At the telescope's 6.5 m primary mirror the subapertures are 54.2 cm on a side. This geometry produces 108 subapertures which are at least 50% illuminated, resulting in 216 slope measurements. The actual lenslet array was manufactured by Adaptive Optics Associates (AOA) and consists of a 50 × 50 square array of epoxy lenses stamped from a precise master and mounted on one side of a 6 mm thick, BK7 glass substrate. From this array the best 12 × 12 lenslet group was chosen. The lenses have a focal length of about 3.4 mm and a 144 μm pitch, which is commensurate with a 6 × 6 subarray of CCD pixels. For an unaberrated input wavefront in the visible, each lens produces a spot on the CCD which has a FWHM of about 13 μm, so the spot is slightly larger than a single pixel.

In normal operation at the MMT, our use of quad-cells for the 12 × 12 subapertures translates to 3 × 3 binning with no guard pixels over the 80 × 80 CCD. There will be four quad-cell subapertures straddling the obscuration of the pupil by the hole in the primary mirror. The 589nm laser for the sodium laser guidestar will be projected to 90 km altitude sodium layer from a central position behind the secondary mirror. With four quad-cells straddling the pupil obscuration instead of a single quad-cell centered on and covering the pupil obscuration, we eliminate most of the scattered light to the central subapertures of the WFS due to Rayleigh scattering in the lower atmosphere. If we had chosen 13 × 13 subapertures instead of 12 × 12 subapertures, then we would have covered the central obscuration with a single subaperture, and Rayleigh scattered light would be more of a nuisance. Also, with 13 × 13 subapertures and four port readout of the CCD, a significant number of the quad-cells would have their pixels read out by multiple ports, which could easily introduce errors due to different gains and biases of the different ports. With 12 × 12 subapertures and 3 × 3 binned quad-cell pixels, each quad-cell is read out by only one of the four CCD ports. We summarize the MMT WFS configuration in Table 1.

Pupil Size	6.5 meters
Subaperture Size	0.542 meters
Plate Scale	60 μm/arcsec
CCD Type	EEV CCD39A, 80 $\times$ 80 four-port frame transfer
CCD Unbinned Pixel Size	24 μm $\times$24 μm
CCD Binning	3 $\times$ 3
CCD Total Noise	4.5-5.0 electrons
Maximum CCD Frame Rate	625 Hz (1.596 ms read time, 1.600 ms integration time)
Minimum CCD Pixel Time (3 $\times$ 3 binning, double sample)	5.86 μs
CCD Frame Transfer Time	27.2 μs
Lenslet Type	AOA precision-stamped epoxy
Subaperture Type	2 $\times$ 2 quad-cells
Number of Subapertures	12 $\times$ 12 = 144 (108 illuminated)
Lenslet Focal Length	3.4 mm
Lenslet Pitch	144 μm
Lenslet Position	glued to CCD package (no relay optics)
Subaperture Angular Size	$\pm$1.25 arcsec or $\pm$5 waves of tilt (at 0.589 nm)
WFS spot size (0.7 arcsecond seeing, estimated)	43 μm FWHM or 0.72 arcseconds
Slope Transfer Curve Gradient (Diffraction Limited, measured)	1.33 per wave of tilt (both directions)
Slope Transfer Curve Gradient (0.7 arcsecond seeing, estimated)	0.55 per wave of tilt (0.60 for "perfect" pixels)
Slope Transfer Curve Unsaturated Dynamic Range (0.7 arcsecond seeing)	$\pm$2 waves of tilt or $\pm$0.50 arcseconds
Slope Transfer Curve Saturated Range (0.7 arcsecond seeing)	$\pm$3 waves of tilt or $\pm$0.75 arcsecond (without subaperture cross-talk)

Table 1. MMT WFS parameters

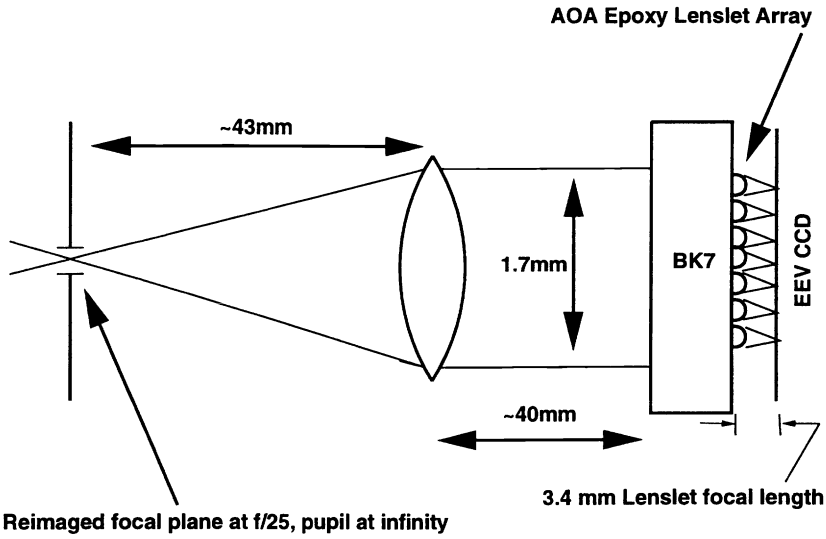

Figure 2. A sketch of the MMT WFS geometry (not-to-scale), showing the 2.5 arcsecond field stop in the $f/25$ focal plane, the lens to form a pupil, and the lenslet array glued in close proximity to the CCD chip. plane

lenslet center with respect to quad-cell center	(xy-translation)	± 5 μm
lenslet xy-axes with respect to CCD xy-axes	(xy-rotation)	$\pm 0.5°$
lenslet plane with respect to CCD detector plane	(z-tilt)	$\pm 5.0°$
lenslet-to-detector separation with respect to lenslet focal length	(z-translation)	± 50 μm
illuminating beam collimation		$\pm 0.5°$
illuminating beam FWHM		> 3 mm

Table 2. Tolerances for the WFS lenslet and CCD alignment. All of the specifications, except the last, are upper limits. The coordinate system for these tolerances uses the detector plane as the xy-plane with z pointing out of the detector.

2. ASSEMBLING THE WAVE FRONT SENSOR COMPONENTS

A unique feature of the WFS for the MMT's AO system is that the lenslet array was bonded directly to the CCD package, thus avoiding the need for any reimaging optics, as sketched in Figure 2. To our knowledge our approach of gluing a commerically available lenslet array directly to the CCD chip housing has never been accomplished before, the closest analog being etching the lenslets onto a CCD cover slide *proposed* by Roland *et al.*[11] While our gluing approach simplifies the WFS hardware, its biggest risk is that after gluing the components together the alignment cannot be adjusted. Therefore, the initial positioning of the lenslet array with respect to the CCD must, by necessity, be very good. The specifications for the gluing procedure are listed in table 2.[12] These tolerances were determined with two basic goals in mind. First, in order to take full advantage of the limited linear region of the WFS transfer curve, the lenslet spots should be within 5 μm of their respective quad-cell centers. Second, in order to maximize the sensitivity of the WFS, the distance from the lenslets to the detector should be within 50 μm of the focal length of the lenslet array. To accomplish the task of gluing the lenslet to the CCD package, a simple optical system was constructed to provide collimated illumination at 0.6328 μm and allow submicron adjustment of the various alignment degrees of freedom.[1]

Before the lenslet could be permanently attached to the CCD, the required height of the lenslet array above the CCD package had to be determined. The measurement of this distance was necessary so a spacer could be made to hold the lenslet at the proper distance from the detector plane. The CCD detector plane was required to be within 50 μm of the lenslet focal plane. Near focus, the size of the lenslet spots was about the size of one CCD pixel, so

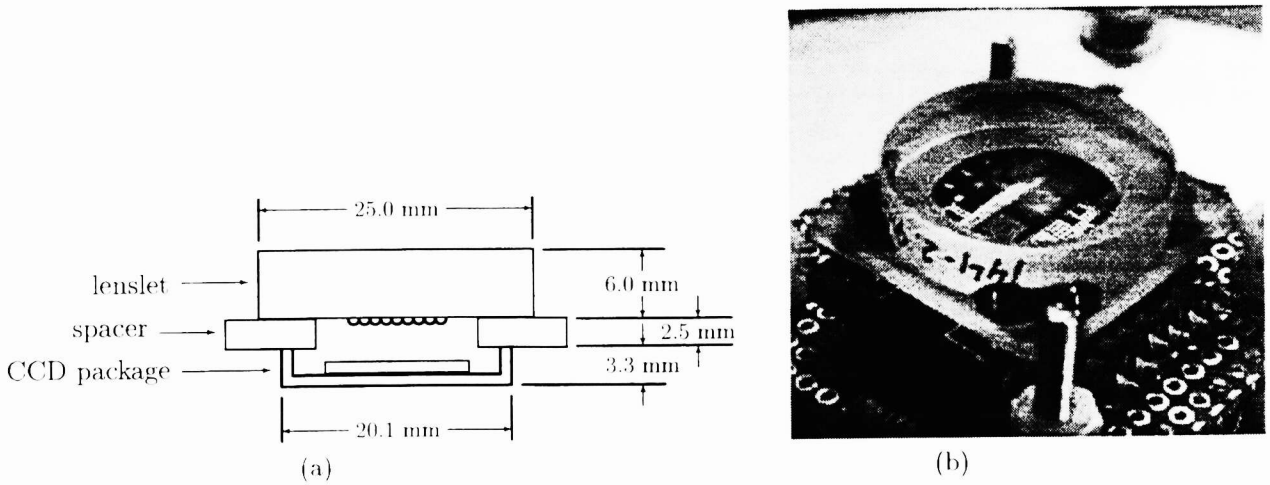

Figure 3. An assembled WFS after the lenslet has been bonded to the CCD package. Figure (a) displays a cross sectional diagram of the CCD, spacer, and lenslet. Figure (b) shows the WFS after assembly. The spacer for the WFS shown is made of BK7.

determining the correct position visually by simply looking at CCD images, was difficult. Therefore, to determine the proper spacer thickness, CCD data were recorded at several lenslet height positions. After each change in height, the lenslet alignment was adjusted so the focused spots were centered on individual pixels. Once the alignment was fine tuned, 50 CCD images were collected and averaged. An intensity distribution factor (IDF) metric was calculated as the ratio of the sum of the counts in the 8 pixels surrounding the peak pixel in each subaperture relative to the counts in the peak pixel. The IDF metric should be at a minimum at the desired lenslet height; therefore, from the lenslet height at IDF minimum, the thickness of the spacer was chosen to be 0.100 inches (2.54 mm).

After the proper CCD-lenslet separation was determined, a steel washer with the desired thickness was obtained for use as the spacer. Using an epoxy recommended by the CCD research group at Steward Observatory, the lenslet was glued to the washer.* After the epoxy was fully cured, a process which took about 24 hours, the lenslet was placed back into its alignment bracket. Before gluing the spacer to the CCD package, the lenslet alignment was adjusted so the focused spots were centered on the subaperture quad-cells. Once the alignment was fine tuned, two small dots of epoxy were placed on each side of the CCD package at the junction with the spacer. For the next several hours while the epoxy cured, the alignment of the CCD and lenslet array was monitored and adjusted as necessary.

Roughly twenty four hours after the epoxy was first placed on the CCD package, the alignment bracket was removed from the lenslet array. Pictures of an assembled WFS are given in figure 3. The final alignment between the lenslet and CCD is demonstrated in figure 4. The WFS image shown in the figure was obtained after averaging 90 WFS frames and applying dark and flat correction. The vector plot shows an estimate of the residual centroid offsets for the focused spots in each subaperture. The randomness of the offset vector orientations is evidence the best alignment was achieved. Due to a shadowing effect by the CCD frame transfer mask which affected the top 3 rows of the CCD, the offsets for the top row of subapertures were ignored and set to zero in the vector plot.† Initially the worst offset vector was 2.73 μm long. However, after the average xy-offset was removed, about 0.25 μm in each axis, the worst offset was only 2.50 μm, the mean was 0.90 μm, and the rms was 1.05 μm.

Using the calculated offsets and a least-squares reconstructor, the residual wavefront profile was estimated. For a wavelength of 0.6238 μm, the residual phase error was calculated to be 0.267 radians, resulting in a Strehl reduction factor of 0.93. In the H band (λ = 1.65 μm) the Strehl factor is 0.99, an excellent result. If desired, the Strehl

*The adhesive was selected based on past CCD research. It was shown to make reliable silicon to Kovar bonds down to LN2 temperatures, and the bonds held through many cycles between room temperature and LN2. It was also shown to be non-electrically conductive.

†The frame transfer mask was created by depositing aluminum directly onto the CCD detector plane. The process used to deposit the aluminum is difficult to control so the edges of the mask were not sharp.

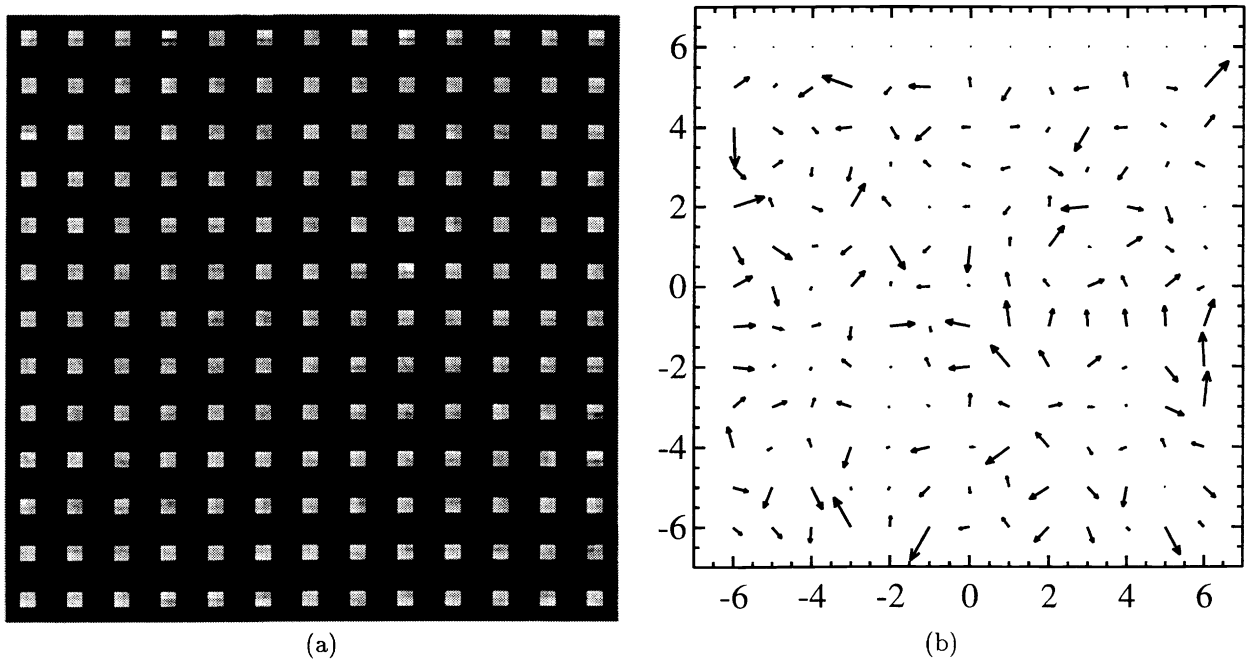

Figure 4. Wavefront sensor alignment after the lenslet was bonded to the CCD package. Figure (a) shows the unbinned WFS image; each spot in this CCD image is in fact a 2×2 quad-cell with each of the four pixels nearly evenly illuminated. Figure (b) shows the estimated centroid offsets for the spots in each subaperture. The largest offset is 2.50 μm and the mean offset is 0.90 μm. The units for the axes in figure (b) are subapertures, where one subaperture is 144 μm across. However, the vectors have been scaled so the longest vector has a length of 1.0 on the graph.

reduction can be compensated for during AO system operation by subtracting the baseline offsets from the WFS output.

After assembling this first prototype WFS, an important oversight in the construction was recognized. The problem had to do with the mismatch in the coefficient of thermal expansion (CTE) between the component materials. While the steel spacer has a CTE of about 12 ppm/°C, the lenslet substrate, which is made of BK7 glass, and the CCD chip carrier, which is made of gray alumina, have CTE's of 7.1 and 6.7 ppm/°C, respectively. The CTE differences would cause very large stresses to build up in the materials if the WFS package were cooled down to its operating temperature of -50°C. Although the steel and epoxy are able to withstand fairly large stresses, the lenslet and chip carrier cannot, and it is possible they would fracture before the epoxy bonds gave out. Not only would this destroy the superb WFS alignment, it would be costly to replace the lenslet or CCD should they fracture. Fortunately this problem can be remedied by simply using a different material for the spacer, such as BK7, as we have done for the final WFS. Very recently, we cooled the bonded CCD and lenslet array down to -50°C for the first time. Judging from the WFS output images taken before cooling, at the coldest temperature, and after warm-up, the bonding appears to have survived the temperature cycle, which means we properly matched the CTE's for the three different pieces (CCD package, spacer and lenslet substrate). Additionally, temperature cycle does not drastically affect the lenslet/CCD alignment, except for the need to take dark images at the different temperatures.

3. INITIAL WAVE FRONT SENSOR TESTING

A series of four experiments were performed with the prototype WFS in order to determine its expected performance. The first two experiments were performed before the lenslet and CCD were bonded together. We measured the innate CCD read noise, and we examined the crosstalk between neighboring CCD pixels. The crosstalk data was then used to estimate the WFS transfer curves under different conditions. The third test confirmed the estimation results from the second experiment by actually measuring the WFS transfer curves after the WFS components were assembled.

In the fourth experiment, we measured the WFS slopes for a static turbulence plate placed in front of the WFS camera.

3.1. Measurements of CCD Noise

We are required to place our WFS camera at the MMT on a stage which is dynamically rotatable about the optical axis and dynamically translatable by ~10 cm in focus. This restricts camera space, access , and weight. This means:

- liquid nitrogen cooling is difficult to implement, and
- a five foot cable is required to connect the CCD to the CCD controller.

These constraints make it non-trivial to make the CCD system noise and the thermal noise negligible, though the innate CCD read noise should remain unaffected.

The requirement for the dynamically rotatable WFS stage comes from the following argument. In an ALT-AZ telescope like the MMT, the focal plane instrument plane needs to be derotated to compensate for the rotation of the sky during a long observation. Therefore, our adaptive optics system for the 6.5 m MMT with adaptive secondary needs to have the wavefront sensor camera on a dynamically rotatable stage with respect to the telescope focal plane so that the registration of the wavefront sensor camera subapertures does not change with respect to the actuators behind the adaptive secondary mirror as the telescope focal plane is derotated during the observation. The substantial focus translation requirement for the WFS camera at the MMT stems from the variation of the apparent sodium layer height with zenith angle and also from the need to switch between natural guidestar AO and sodium laser guidestar AO. Such variability in object distance means that the longitudinal position of the image of the pupil on the WFS lenslet array will vary by ~10 cm.

At liquid nitrogen temperatures, we have measured 3.5–4 electrons of CCD amplifier read noise *without* a cable connecting the dewar to the CCD controller, which agrees with EEV's manufacturing specification of 3.7 electrons at our 170 kHz pixel rate. Since liquid nitrogen cooling was not allowed, we initially tried a two-stage thermoelectric cooler. Two-stage thermolectric cooling was not able to reduce the thermal dark current of the camera for 1 millisecond exposures below 5 electrons. Therefore, we chose to cool the CCD with a three-stage thermoelectric cooler, which provided −50°C cooling and allowed us to achieve 1 electron/millisecond dark current.

Our final read rate is 5.86 μs per 3×3 binned pixel per port (2 ADC reads each of 1.9 μs plus 2.06 μs of overhead). With 27.2 μs frame transfer, 37.6 μs clearing of the serial line, 0.68 μs skipping of 1 unused row, 26.52 μs for the 3×3 binning (13 times), 4 μs of overhead, we get 1.596 millisecond latency per frame, or 626.6 Hz maximum frame rate, with only 2% smearing by the 27.2 μs frame transfer. With the current Gen II SDSU controller without an external clock, frame times must be an integer multiple of 800 μs, so the 1596 μs latency is almost precisely consistent with this frame time constraint. We need only to add 4 μs of delay to be self-consistent, and hence our final frame rate will be 625 Hz.

For a long time, we have had troubles with sporadic and non-repeatable system noise, sometimes reaching 10–20 electrons in intensity. This is caused by a combination of factors: the 3–5 foot cable needed to connect the WFS camera to the SDSU/Leach GenII controller (due to the necessity of the rotary stage), and what appears to be 50MHz electromagnetic waves emanating from the GenII controller (not seen in the GenI controllers). This system noise problem largely disappears when the shorting test plug from the video line to ground at the end of the cable is either well-shielded, or when the CCD is attached to the cable, as in operation. The total noise in the final 3-stage thermoelectrically-cooled dewar is now 4.5–5.0 electrons, which is lower than Gemini's read-only noise of 5.3 electrons with similar EEV CCD39A chip,[10] for an *unbinned* 3.1 millisecond frame readout time. Our total noise can be reduced to 3.6–3.8 electrons by increasing the pixel ADC integration time from 2 μs to 5 μs, but this effectively doubles the CCD read latency/frame. The total noise in a liquid nitrogen cooled dewar without a cable was 3.5–4 electrons, so the addition of the system noise from the new dewar and the cable, and the addition of the dark current from the warmer chip temperature, together only added at most 1.5 electrons of noise, which is somewhat substantial, but manageable. The 4.5–5.0 electrons total noise is a major step towards our goal for the total CCD noise to be around 3 electrons, which would maintain the highest signal-to-noise ratios for atmosphere-aberrated slopes measured with 9th magnitude sodium laser guidestars at 1kHz frame rate.[13]

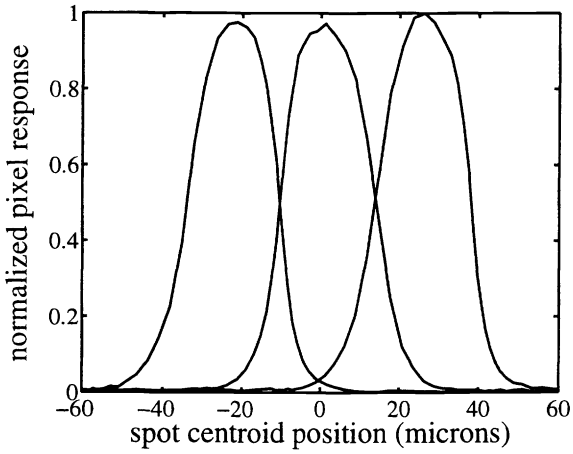

Figure 5. Normalized pixel response curves in the serial direction for three adjacent CCD pixels showing the amount of crosstalk between pixels. Each pixel is 24 μm wide.

3.2. Pixel Crosstalk and WFS Transfer Curves

Crosstalk (or blur) between neighboring CCD pixels degrades the performance of the WFS. In order to get a handle on the amount of pixel crosstalk in the WFS CCD and its effect on the performance of the WFS, two complementary experiments were carried out. The first experiment was done before the WFS components were glued together and the second was done after. The first experiment examined the CCD pixel crosstalk by moving a small, focused laser spot along the rows and columns of the CCD and recording the response of the illuminated pixels. The collected data were then used to estimate the WFS transfer curves. The second experiment directly measured the transfer curves of the assembled WFS described above by changing the incidence angle of a collimated laser beam falling on the WFS. A comparison of the results from these two experiments is presented below.

The setup for the first experiment was simple. A collimated HeNe laser beam at 0.6328 μm was created using a spatial filter assembly and an achromatic doublet. A portion of this beam was then focused onto the WFS CCD using an infinity-corrected microscope objective which had a 5.0 mm focal length and 3.0 mm aperture. The microscope objective was placed in front of the CCD on a translation stage which allowed the objective to be moved laterally with a resolution of 1 μm. The distance between the objective and the CCD was controlled by a second translation stage. A variable aperture was used to limit the size of the beam entering the objective to a diameter of about 1.5 mm. Initial measurements taken without this aperture indicated a problem with scattered light falling on the detector. The aperture eliminated this problem. It also increased the FWHM of the focused spot from 1.1 μm to 2.2 μm.

Focusing of the laser on the CCD was accomplished with the help of a telescope focused at infinity. Some of the light falling on the CCD detector surface was reflected back through the microscope objective. While viewing this reflected light through the telescope, the separation between the CCD and objective was adjusted until an Airy spot was observed, indicating proper focus. Once the system was aligned, the laser spot was moved across a row or column of CCD pixels at 2 μm intervals and images were recorded at each position. For this discussion, a CCD row is defined by the serial readout direction of the CCD data and a column is defined by the parallel readout, or frame transfer, direction. The readout directions are indicated in figure 1. Figure 5 shows the pixel response for three adjacent pixels. This figure can be thought of as the probability that a photon will register in pixel n if it lands at position x. The amount of crosstalk between pixels is significant. For instance, a photon that lands 6 μm, or one quarter of a pixel width, from the center of a CCD pixel has about a 12% chance of registering in the adjacent pixel whose center is 18 μm away.

After deconvolving the shape of the focused spot from the pixel response data, the pixel transfer functions were calculated from the energy imbalance for neigboring pixels: $PTF = (I_1 - I_2)/(I_1 + I_2)$. The average, normalized pixel transfer functions, showing the energy imbalance between pixels as a function of spot location, are displayed in figure 6. The transfer functions that would have been obtained with perfect pixels having no crosstalk are also shown in the figure. Since the MMT AO system will bin the CCD pixels by a factor of 3 in order to increase the

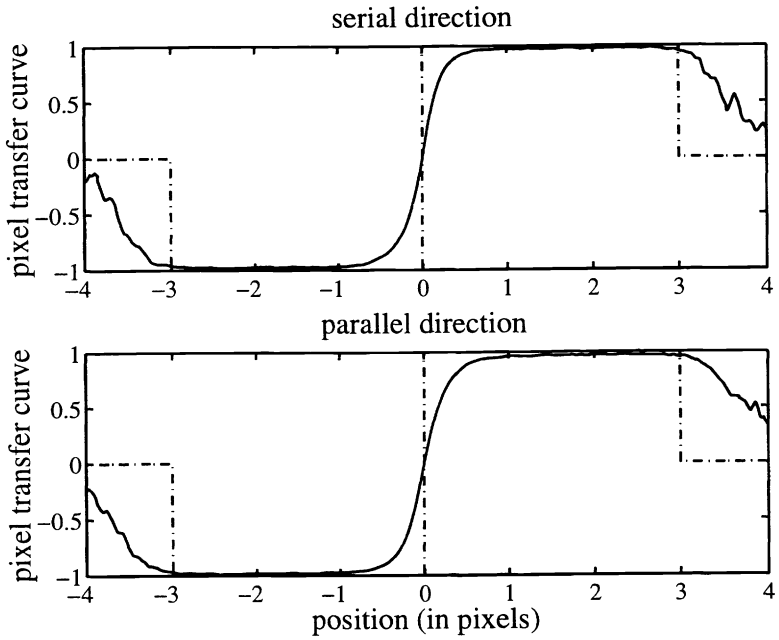

Figure 6. Pixel transfer curves between CCD pixels after binning by a factor of 3. The dashed line is for a perfect CCD with no pixel crosstalk and the solid line was calculated from the measured pixel responses. The top (bottom) graph shows the transfer curves for the serial (parallel) readout direction of the CCD. The units for the x-axes are pixel widths. The pixels are 24 μm across.

readout rate and reduce the effects of read noise, binning has been accounted for in this calculation. The slow rolloff and noisiness of the curves at the edges of the graphs were a result of division by the total number of counts in the pixels, which was small and noisy at the plot edges. In the serial readout direction, the slope of the transfer curve at the quad-cell boundary is 0.218 per micron of centroid offset. In the parallel direction it is 0.167 per micron. The slopes are slightly different in the two directions because of the three-phase integration scheme required by this CCD, which caused the boundary between pixels in the parallel readout direction to be fuzzier than in the serial readout direction.

Using the above results, the expected WFS transfer curves were estimated. The WFS transfer curve is defined as the relationship between the incident wavefront tilt and the resulting energy imbalance sensed by the WFS. This function can be calculated by convolving the average point spread function (PSF) of the WFS subapertures with the CCD pixel transfer curves. This operation produced the curves shown in figure 7. The average PSF for this calculation was estimated by the theoretical, focal-plane, diffraction pattern created by the square WFS subapertures. Since the MMT AO system is expected to operate with a sodium laser guide star, the PSF was calculated for a wavelength of 0.589 μm so the FWHM of the focused spot was 12.3 μm, or a 0.20 arcseconds image-width. These curves give the upper limit on the quad-cell performance since, in the presence of turbulence, the focused spots on the WFS will be somewhat larger than the diffraction limit. Once again, due to the CCD integration scheme mentioned above, the transfer curves are slightly different in the two directions, with the transfer curve gradients in the serial direction of 1.33 per wave of tilt, and in the parallel direction of 1.24 per wave of tilt, or a ratio of 1.07. The GenIII WFS at Starfire Optical Range reports a bigger asymmetry between the parallel and serial slope transfer curve gradients ($1.2/1.0 = 1.20$).[7]

In the presence of uncorrected turbulence at the MMT, a more reasonable estimate of the focused WFS spots is a Gaussian with a FWHM of about 43 μm, corresponding to 0.7 arcseconds seeing. Transfer curves based on this model for the WFS spots are shown in figure 8. Compared to the diffraction limited case, the discrepancy between the curves for perfect pixels and actual pixels is much less, indicating crosstalk between pixels is less of an issue. However, since the WFS's sensitivity is proportional to the slope of the transfer curves at the quad-cell center, the larger spot size also reduces the sensitivity of the WFS. Unfortunately, the loss in sensitivity is unavoidable since it

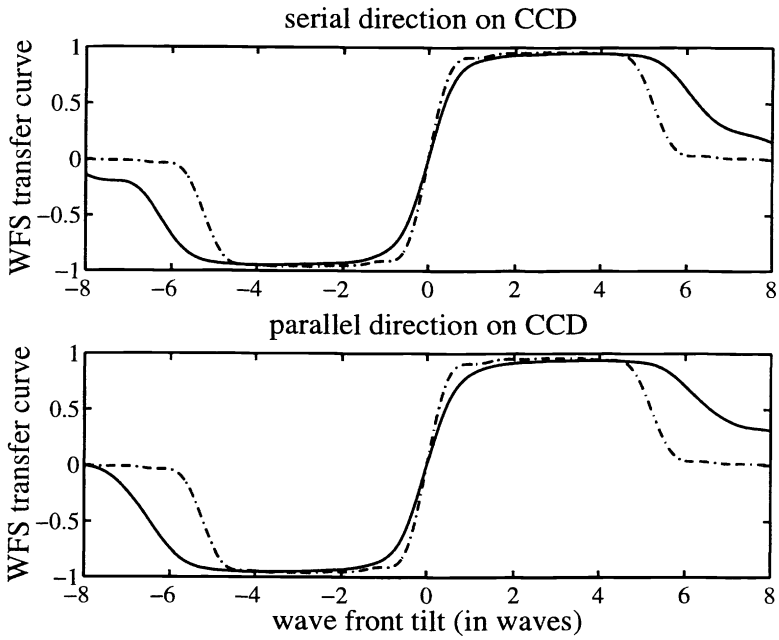

Figure 7. Estimated WFS transfer curves for a pixel binning factor of 3, assuming a diffraction limited PSF for the WFS subapertures. The dashed line is for a perfect CCD with no pixel crosstalk and the solid line was calculated from the measured pixel responses. The top (bottom) graph shows the transfer curves for the serial (parallel) readout direction of the CCD. The units for the x-axes are waves of tilt across a WFS subaperture at 0.589 μm. The gradients at zero tilt are 1.33 and 1.24 per wave of tilt, giving a 7% asymmetry between the two directions.

is dependent on atmospheric conditions.

The curves in figure 7 level off at about 2 waves of tilt, indicating the focused spot is mostly on one side of the quad-cell for tilts greater than this value. At roughly 5 waves of tilt, the spot centroid will be on the boundary between two subapertures. Therefore, the dynamic range of the WFS will be about ± 3 waves of tilt per subaperture at best. Tilts greater than this will produce crosstalk between neighboring subapertures. At the MMT, the expected wavefront tilt over a single subaperture at visible wavelengths is 1–2 waves in median seeing and 2–3 waves in lousy seeing. However, since the AO system will be operating in closed loop at a bandwidth between 50 and 100 Hz, the WFS will rarely see tilts greater than one wave except at system startup and during the worst seeing conditions. Therefore, crosstalk between subapertures should generally not be a problem once the AO loop is closed and stable.

After we glued the WFS lenslet array to the CCD, we directly measured the WFS transfer curves by changing the tilt of a wavefront incident on the lenslet array and recording the WFS outputs. A Physik Instruments (PI), 2-axis fast steering mirror was placed in a one inch diameter collimated laser beam at an angle of 45 degrees. The mirror was computer operated and was used to direct the laser beam onto the WFS and to control the beam's angle of incidence. The angular resolution of the steering mirror was about 1 μrad. Unfortunately, its angular range was only about 4 mrad, which was only enough to move the spots on the WFS CCD about half of a pixel. Therefore, an afocal lens system with a transverse magnification around 0.1 was placed between the steering mirror and the WFS. With this relay system each lenslet spot could be scanned across most of its respective CCD subaperture.

After the system was setup and operational, the alignment of the components was fine tuned. The alignment was set so the WFS spots were centered on the appropriate CCD quad-cells when the actuator commands for the PI mirror were zero. Once this alignment was accomplished, transfer curve data were collected for the serial and parallel readout directions of the WFS CCD. During setup the tip-tilt axes of the PI mirror had been aligned with the rows and columns of the CCD. Therefore, to scan the incident angle of the laser beam along one WFS direction, the tilt command for one of the PI mirror's axes was stepped from one end of its range to the other while the actuator command for the other axis was held constant. During the scan, the mirror paused at 151 uniformly spaced tilt

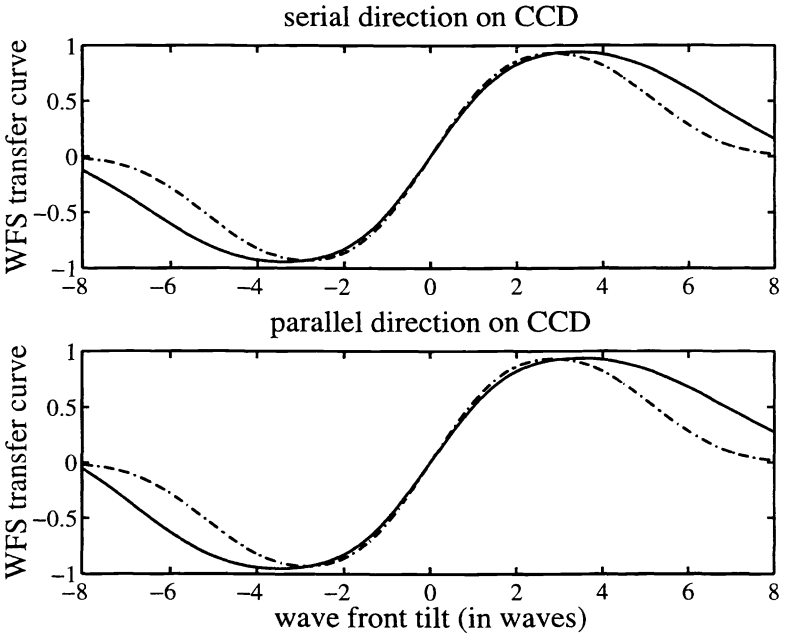

Figure 8. Estimated WFS transfer curves in the presence of 0.7 arcsecond seeing for a pixel binning factor of 3. A Gaussian WFS spot with a FWHM of 43 μm was used to calculate the curves. The dashed line is for a perfect CCD with no pixel crosstalk and the solid line was calculated from the measured pixel responses. The top (bottom) graph shows the transfer curves for the serial (parallel) readout direction of the CCD. The units for the x-axes are waves of tilt across a WFS subaperture at 0.589 μm. The gradients at zero tilt are tabulated in Table 3, but there is clearly very little (less than 10%) degradation in the gradients from the ideal case of perfect pixels.

positions in order for 200 unbinned WFS images to be collected and averaged. The same procedure was used to collect data for the other WFS direction, but the roles of the PI actuators were reversed. In order to simplify the data collection process, a computer program was written to coordinate the scanning of the steering mirror and the collection of WFS images.

The WFS transfer curves were calculated from the average images collected using the above procedure. The results of this calculation for a binning factor of three are shown in figure 9. To obtain these plots, the transfer curves for each subaperture were independently calculated. The average transfer curves were then determined by averaging the individual curves. For comparison, transfer curve estimates based on the data collected during the second experiment is also shown in the figure. These estimated curves were calculated for a diffraction limited spot at a wavelength of 0.6328 μm. The agreement between the estimated and measured curves is quite good. The level of agreement validates the other results derived from the second experiment.

An analysis of the transfer function data shown in figures 6–9 is given in table 3. The table lists the gradients of the WFS transfer curves at the quad-cell center for perfect pixels and the measured pixel responses. The table also lists the WFS noise sensitivity which is defined as the inverse of the gradient. This parameter is important because the WFS measurement uncertainty is directly proportional to the noise sensitivity.[13,14] As shown in the table, the noise sensitivity has an ideal, lower limit of 0.5 in the diffraction limited case. In real life, this limit will never be reached for two reasons. First, atmospheric turbulence will cause the WFS spots to be larger than the diffraction limit. Second, real CCD pixels are never "perfect." Both of these factors will increase the WFS's sensitivity to noise.

The gradients for the measured transfer curves listed in table 3 represent a marked improvement over similar results reported for a currently operating AO system at the Starfire Optical Range (SOR).[7] That system reported gradients of 1.5 and 1.3 for WFS transfer curves estimated by a method similar to the pixel-crosstalk experiment presented above. Due to alignment errors between the lenslet and CCD at SOR, the actual measured transfer curve gradients of 1.2 and 1.0 were significantly worse than the predicted gradients (from pixel-crosstalk alone) of 1.5 and

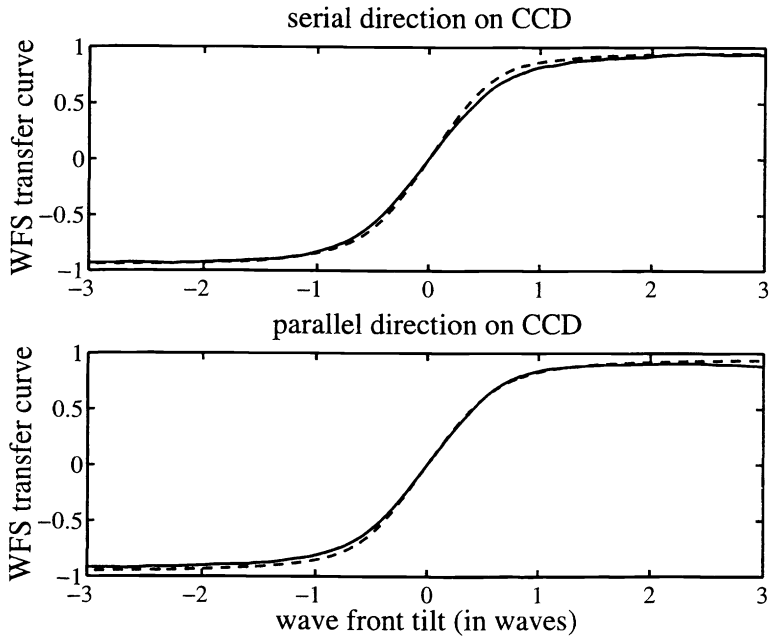

Figure 9. Measured WFS transfer curves in the absence of uncorrected turbulence for a pixel binning factor of 3. The solid line is the measured transfer curve from the second experiment and the dashed line is the estimated curve based on the data from the second experiment. The top (bottom) graph shows the transfer curves for the serial (parallel) readout direction of the CCD. The units for the x-axes are waves of tilt across a WFS subaperture at 0.6328 μm. Note that the calculation agrees well with the measurement, which means that our alignment and gluing was accurate. The slope transfer curve gradients are tabulated in 3.

1.3. Our measured transfer function gradients of 1.33 are *not* lower than the predicted gradients, and our measured gradients are higher than those measured at SOR. Therefore, bonding the lenslet and CCD together, as we have done, avoids the reduction in transfer curve gradient observed in the non-bonded GenIII WFS camera at SOR.

3.3. Known Incident Wave Front

This last experiment used our high-quality, inexpensive oil-filled prototype turbulence plate[15] to create a known static phase profile at the WFS. Then WFS images were recorded and the data used to reconstruct an estimate of the wavefront.

This test was also performed after the WFS had been placed in the laboratory AO system.[16] It seemed reasonable to use the laboratory system for this test since the alignment and magnification between the entrance aperture and the WFS were well defined. Before placing the turbulence phase plate into the system, the AO loop was closed around the system optics in order to compensate for any system aberrations and null the WFS outputs as best as possible. At this point the phase plate was placed into a 24 mm diameter, collimated laser beam ($\lambda = 0.6328$ μm). At the WFS the beam diameter was reduced by a factor of 20.75 so the beam almost completely covered the central 7×7 grid of subapertures of the WFS, with the exception of the 4 subapertures in the corners of the grid. Figure 10 shows the WFS images obtained with and without the *static* turbulence phase plate in the system. The CCD pixels were not binned in this test in order to increase the dynamic range of the measurements.

From the WFS image data, the wavefront slopes were calculated from the 6×6 pixel quad-cells. The slopes were easily calculated for the image recorded without the phase plate in the system. However, some adjustments were required in order to accurately calculate the slopes for the image recorded with the phase plate in the system. Figure 10(c) shows the major aberration introduced by the turbulence plate was global tilt. In fact, this tilt was large enough to create crosstalk between adjacent subapertures. In order to produce more accurate results, the 6×6 pixel groups which made up the subapertures were shifted two pixels to the left and one pixel down. While this did not completely solve the crosstalk problem, as seen in the subaperture in the third row from the bottom and

	transfer curve gradient		noise sensitivity	
	serial (x)	parallel (y)	serial (x)	parallel (y)
estimated curves for zero size spot				
"perfect" pixels	∞	∞	0	0
measured pixels	3.00	2.30	0.332	0.435
estimated curves for diffraction limited spot at 0.589 μm				
"perfect" pixels	2.00	2.00	0.500	0.500
measured pixels	1.33	1.24	0.750	0.808
measured curves for collimated input beam at 0.6328 μm				
"perfect" pixels	2.00	2.00	0.500	0.500
measured pixels	1.33	1.34	0.753	0.744
estimated curves for 0.7" seeing at 0.589 μm				
"perfect" pixels	0.60	0.60	1.661	1.661
measured pixels	0.56	0.55	1.780	1.803

Table 3. The WFS transfer curve gradients at the quad-cell boundaries and the resulting noise sensitivity. Results are listed for the transfer curve estimated in the first experiment and measured in the second. The units for the gradients are change in WFS output per wave of tilt across the subaperture. The CCD pixels have been binned by a factor of 3.

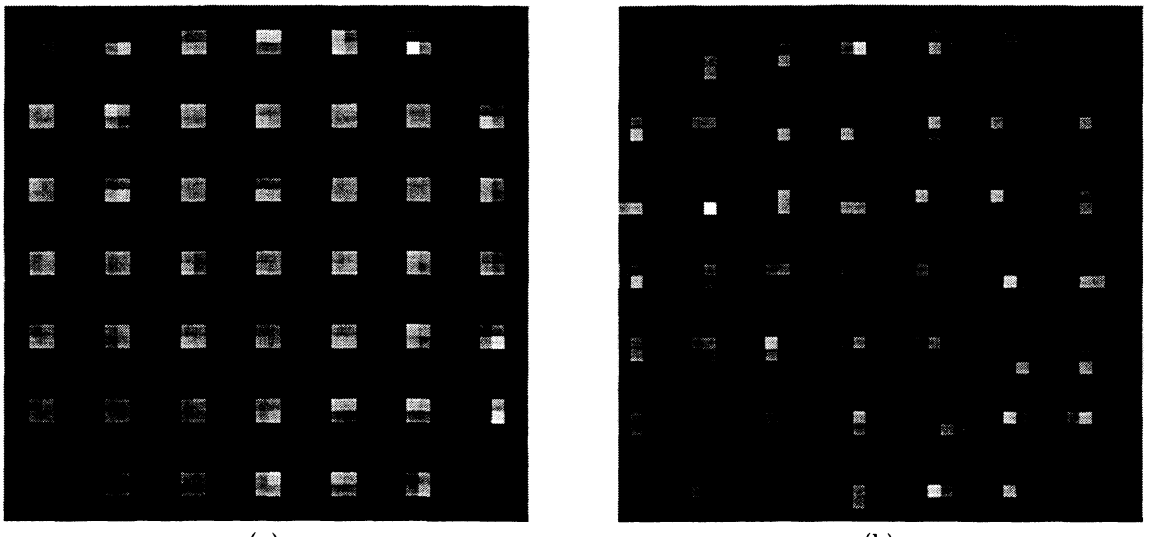

(a) (b)

Figure 10. WFS images with and without the turbulence phase plate.

second column from the right, it eliminated most of it. The effect of the phase plate on the WFS was then isolated by subtracting the two sets of slopes and removing the global tilt. We have used such WFS signals to close the loop around static turbulence in a benchtop 37 actuator AO system.[16]

4. CONCLUSION

By gluing the lenslet array permanently to the CCD package, we achieve and forever maintain near perfect lenslet-CCD registration, so that there is no flexure, thermal creep, or transfer curve gradient degradation. Also, since the lenslet pitch is exactly matched to the CCD pixels and with the direct gluing, we eliminate the need for relay optics. The residual misregistration ($\sim$ 1–2 μm) of the lenslets (over 144 μm subapertures) with respect to the quad-cell vertices is due to manufacturing inaccuracies in the lenslets and CCD, and are deemed to be negligible with respect

to the $\sim$ 40 μm image spots of a star through typical turbulence. The total CCD noise is 4.5-5.0 electrons per read, which will allow Strehls of greater than 0.8 with a 9th magnitude laser guidestar.

ACKNOWLEDGMENTS

Manny Montoya, Rich Gonzalez, Curt Blair, Charles Bridges, Dave Baxter and Lee Ulrickson provided superb technical support in the construction and testing of this wavefront sensor camera. F. Wildi is supported by a young researcher grant from the Swiss National Fund for Scientific Research. We have been supported by the Air Force Office of Scientific Research under grant #F49620-94-1-0437 and grant #F49620-96-1-0366.

REFERENCES

1. T. A. Rhoadarmer, *Construction and Testing of Components for the 6.5 m MMT Adaptive Optics System.* PhD thesis, University of Arizona, Optical Sciences Center, 1999.
2. G. Rousset, "Wavefront sensing," in *Adaptive Optics for Astronomy*, D. Alloin and J.-M. Mariotti, eds., vol. C423 of *NATO Advanced Study Institute Series*, pp. 115–137, Kluwer Academic Publishers, 1994.
3. R. V. Shack and B. C. Platt, *J. Opt. Soc. Am.* **61**, p. 656, 1971.
4. T. J. Kane, B. M. Welsh, C. S. Gardner, and L. A. Thompson, "Wave front detector optimization for laser guided adaptive telescopes," in *Active Telescope Systems, Proc. SPIE* **1114**, pp. 160–171, 1989.
5. B. M. Welsh, B. L. Ellerbroek, M. C. Roggemann, and T. L. Pennington, "Fundamental performance limitations and comparison of the Hartmann and shearing interferometer wavefront sensors," *Appl. Opt.* **34**, pp. 4186–4195, 1995.
6. J. W. Hardy, *Adaptive Optics for Astronomical Telescopes*, ch. Optical Wavefront Sensors, pp. 135–175. Oxford University Press, Oxford, 1998.
7. T. L. Pennington, D. W. Swindle, M. D. Oliker, B. L. Ellerbroek, and J. M. Spinhirne, "Performance measurements of Generation III wavefront sensors at the Starfire Optical Range," in *Adaptive Optical Systems and Applications*, R. K. Tyson and R. Q. Fugate, eds., *Proc. SPIE* **2534**, pp. 327–337, 1995.
8. J. C. Shelton, T. G. Schneider, D. McKenna, and S. L. Baliunas, "First tests of the Cassegrain adaptive optics system of the Mount Wilson 100-inch telescope," in *Adaptive Optical Systems and Applications*, R. K. Tyson and R. Q. Fugate, eds., *Proc. SPIE* **2534**, pp. 72–77, 1995.
9. J. C. Shelton. Keck Observatory, private communication.
10. B. Leckie and T. Hardy, "Gemini WFS CCDs and controllers," in *Optical Astronomical Instrumentation*, S. D'Odorico, ed., *Proc. SPIE* **3355**, pp. 529–538, 1998.
11. J. J. Roland, J. P. Gaffard, P. Jagourel, C. Boyer, and P. Gosselin, "Adaptive optics: a general purpose system for astronomy," *Proc. SPIE* **2201**, pp. 58–76, 1994.
12. M. Lloyd-Hart. Center for Astronomical Adaptive Optics, Steward Observatory, University of Arizona, private communication.
13. D. G. Sandler, S. Stahl, J. R. P. Angel, M. Lloyd-Hart, and D. McCarthy, "Adaptive optics for diffraction-limited infrared imaging with 8 m telescopes," *J. Opt. Soc. Am. A* **11**, pp. 925–945, 1994.
14. G. A. Tyler and G. L. Fried, "Image-position error associated with a quadrant detector," *J. Opt. Soc. Am.* **72**, pp. 804–808, 1982.
15. T. A. Rhoadarmer, J. R. P. Angel, S. M. Ebstein, M. Lloyd-Hart, M. A. Kenworthy, I. Lanum, M. L. Rademacher, B. C. Fitz-Patrick, and P. C. McGuire, "Design, construction, and testing of a low-cost static and spinning Kolmogorov turbulence plate for adaptive optics simulation," *(to be published)* , 1999.
16. T. A. Rhoadarmer, P. C. McGuire, J. M. Hughes, M. Lloyd-Hart, S. Schaller, J. R. P. Angel, and M. A. Kenworthy, "Laboratory adaptive optics system for testing the wavefront sensor of the new MMT," *Proc. SPIE* **3762**, 1999.